Supplementary Information for "Oceanic eddies induce a rapid formation of an internal wave continuum"

Luwei Yang[1], Roy Barkan[1,2], Kaushik Srinivasan[1], James C. McWilliams[1], Callum J. Shakespeare[3,4], and Angus H. Gibson[3]

[1]*Department of Atmospheric and Oceanic Sciences, University of California, Los Angeles, LA, CA, USA.*
[2]*Porter School of the Environment and Earth Sciences, Tel Aviv University, Tel Aviv, Israel.*
[3]*Research School of Earth Sciences, Australian National University, Canberra, ACT, Australia.*
[4]*ARC Centre of Excellence in Climate Extremes, Australian National University, Canberra, ACT, Australia.*

Supplementary Note 1: Simulation setup

The eddy-only case is modified from the smooth forcing simulations in (1), and we refer readers to that paper for the detailed parameters for setting up the smooth forcing simulations. Here, we focus on 1) the changes made to smooth forcing simulations to create the eddy-only case, and 2) the changes made to the eddy-only case to create the eddy-wave and wave-only cases.

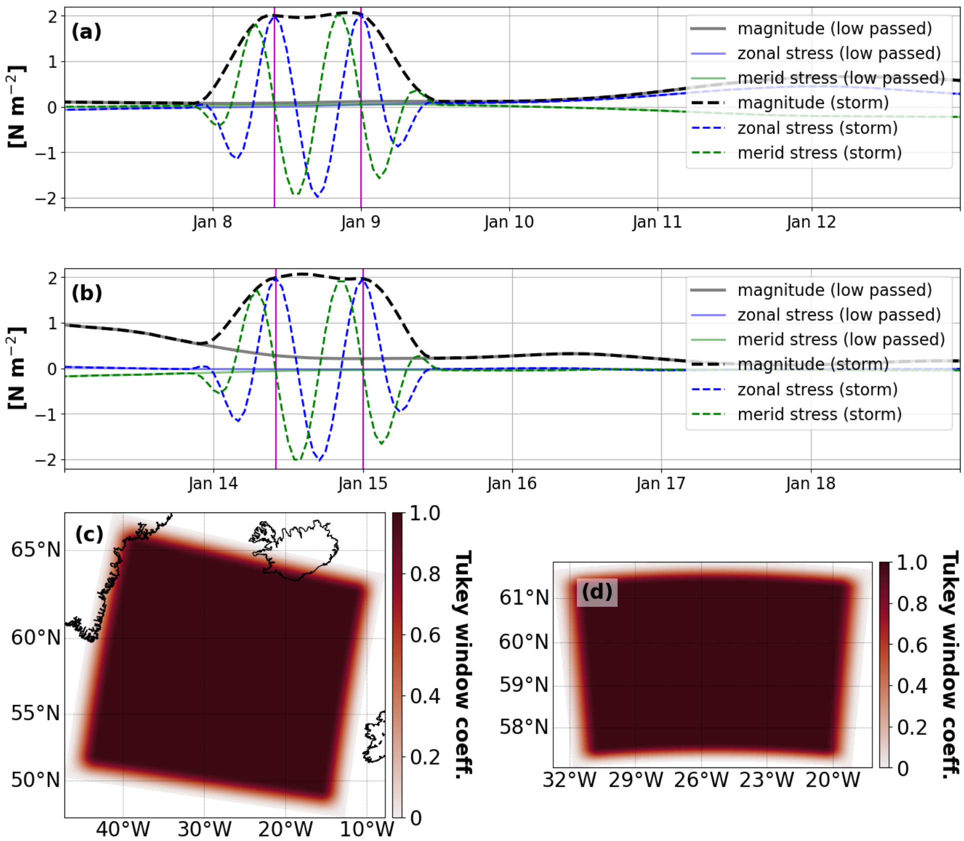

Supplementary Figure 1: The time series of domain-averaged wind stress used to force the (a) 2 km and (b) 500 m simulations, where the solid lines indicate the wind stress in the eddy-only case and the dashed lines the eddy-wave case. The spatial map of Tukey window coefficient applied to the wind stress in the (c) 2 km and (d) 500 m simulations.

The key difference between the eddy-only case and the smooth forcing simulation in (1) is the wind forcing. The eddy-only case is forced directly by wind stress whereas the smooth forcing simulation is forced by the wind velocity. The wind stress used in the eddy-only case is obtained from the smooth forcing simulation by saving the wind stress as an output during the model run; therefore, it is transformed from the wind velocity through bulk formulae (3) and corrected by current feedback (4). The stress forcing approach ensures that the work of the low frequency wind stress is identical between the eddy-only and eddy-wave simulations (Fig. 2a, Supplementary Fig. 4a).

The eddy-wave case is forced by the wind stress (Supplementary Figs. 1a and 1b) that contains a low-frequency component, which is the same as the wind stress used in the eddy-only case, and a resonant component, which lasts for three inertial periods and within each period takes the form

$$\boldsymbol{\tau}(t) = \tau_o \times exp(-ift), \quad 0 < t < T, \tag{1}$$

where $\tau_o = 2$ N m^{-2} and $T = 2\pi/f$ is the inertial period. A symmetric Tukey window is then applied in time to the resonant component, with a shape parameter of 2/3, to guarantee a smooth transition to and from the effective resonant forcing in the second inertial period (bounded by the magenta lines). The use of this smooth transition in the first and third inertial period aims to prevent the generation of high-frequency internal waves due to the abrupt increase or decrease in the wind stress. The resonant component is uniformly added to the entire domain and tapered at four boundaries using a 2D symmetric Tukey window with a shape parameter of 0.2 (Supplementary Figs. 1c and 1d).

The wave-only case is forced by the resonant forcing described above. The restoring temperature and salinity prescribed at the surface are set to be their initial state at the surface. Other flux terms, including surface net heat flux, surface freshwater flux, and short-wave surface radiation, are all set to zero. The initial and boundary conditions are also modified to prevent the generation of eddies. The

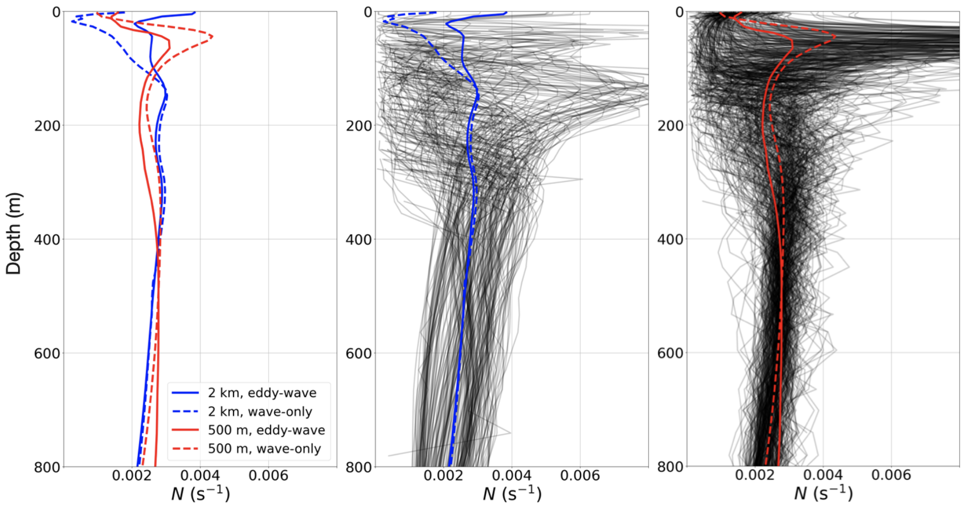

Supplementary Figure 2: (a) The horizontally averaged initial stratification profiles in the eddy-wave and wave-only cases. (b) Initial stratification profiles in the 2 km simulations, where the gray lines indicate the sampled profiles in the eddy-wave case, the blue solid and dashed lines indicate the horizontally averaged initial stratification profiles in the eddy-wave and wave-only cases, respectively. (c) Initial stratification profiles in the 500 m simulations, where the gray lines indicate the sampled profiles in the eddy-wave case, the red solid and dashed lines indicate the horizontally averaged initial stratification profiles in the eddy-wave and wave-only cases, respectively.

temperature and salinity profiles used as the initial condition are obtained as follows. First, interpolate the initial temperature and salinity fields from σ levels to z levels. Then, compute the horizontal average of temperature and salinity at each z level. Finally, assign the horizontally averaged temperature and salinity to all grid points for each z level and interpolate back to σ levels. Note that the temperature and salinity fields are modified to prevent the eddy generation due to the horizontal density difference (i.e., vertical shear). On z levels, this horizontally uniform distribution of temperature and salinity leads to an initial stratification profile that is different from the horizontally averaged initial stratification profile in the eddy-wave case but falls within the spread of the initial stratification profiles sampled across the domain (Supplementary Fig. 2).

Supplementary Note 2: Lagrangian tracks

Lagrangian tracks are sampled at 33 m in the domain from the twelfth hour in day 8 to the twelfth hour in day 12 of the 2 km simulations to illustrate the flow field in the eddy-wave and wave-only cases (Supplementary Fig. 3). Each of these Lagrangian tracks consists of two segments, where the black segment indicates the first half the 4-day time series and the blue the second half. In the wave-only case, the Lagrangian tracks are circular across the domain, demonstrating inertial oscillations in the mixed layer (Supplementary Fig. 3b). In contrast, the Lagrangian tracks in the eddy-wave case are stretched to various extent along different directions, due to the modification of inertial oscillation by eddies (Supplementary Fig. 3a).

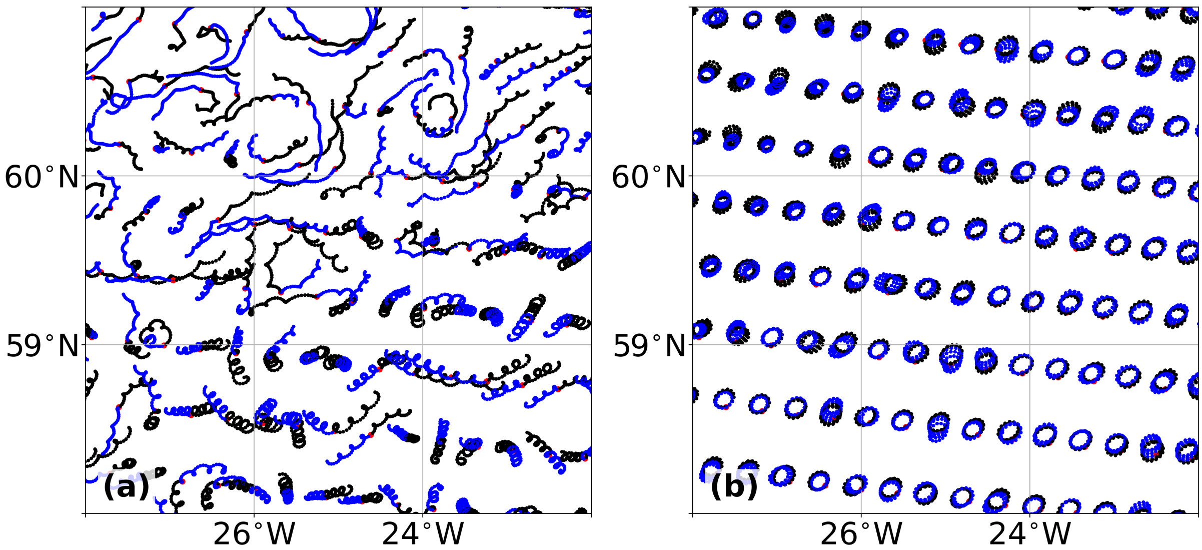

Supplementary Figure 3: The 4-day Lagrangian particle tracks at 33 m sampled every 300 points for the (a) eddy-wave and (b) wave-only cases with 2 km resolution, where the red dots indicate the location of grid points where particles are released, the black and blue segments indicate the tracks obtained from the backward and forward advection with a 2-day time window, respectively.

Supplementary Note 3: Simulated wave field and energy dissipation in the 500 m simulations

The internal wave field in the 500 m simulations (Supplementary Fig. 4) is qualitatively similar to that in the 2 km simulations (Fig. 2). The energy injection by the resonant storm into the near-inertial band is 38.9 mW m^{-2} and 41.6 mW m^{-2} for the eddy-wave case and wave-only case, respectively (Supplementary Fig. 4a). The near-inertial kinetic energy is generated in the mixed layer (Supplementary Fig. 4b), and propagates downward rapidly (Supplementary Fig. 4c). The domain-averaged (in the upper 800 m) internal wave energy dissipation in the eddy-wave case is 1.2×10^{-7} W kg^{-1}, smaller than that in the wave-only case (1.3×10^{-7} W kg^{-1}) due to the unaccounted dissipation below 800 m.

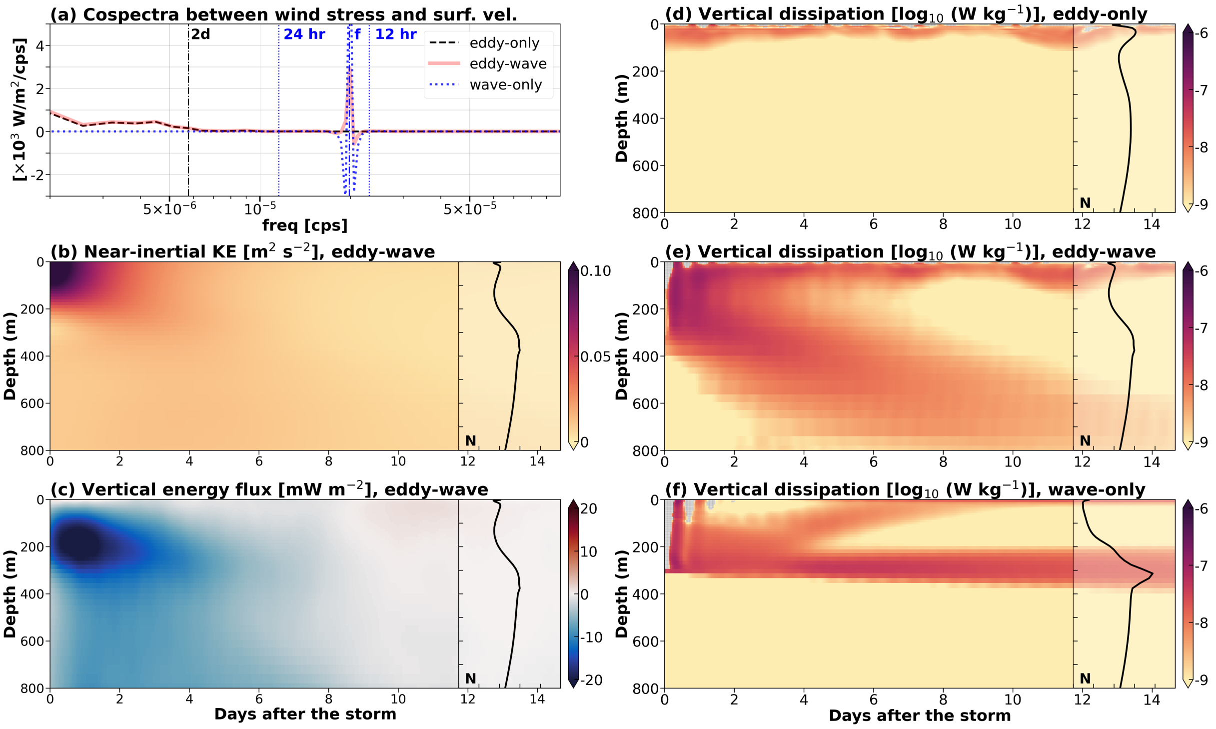

Supplementary Figure 4: Same as Fig. 2 but for the **500 m** simulations.

Supplementary Note 4: Frequency-horizontal-wavenumber spectra in the 2 km simulations

The frequency-horizontal-wavenumber spectra in the 2 km simulations are qualitatively similar to the spectra in the 500 m simulations. In the 2 km simulations, the spectral roll-off occurs at a larger scale (indicated by black vertical dashed lines in Supplementary Fig. 5) and the wavenumber range of the resolved IW continuum is narrower compared with the 500 m simulations. The spectral peaks to the right of the roll-off wavenumber are affected by horizontal numerical diffusion and so their oceanic relevance is unclear.

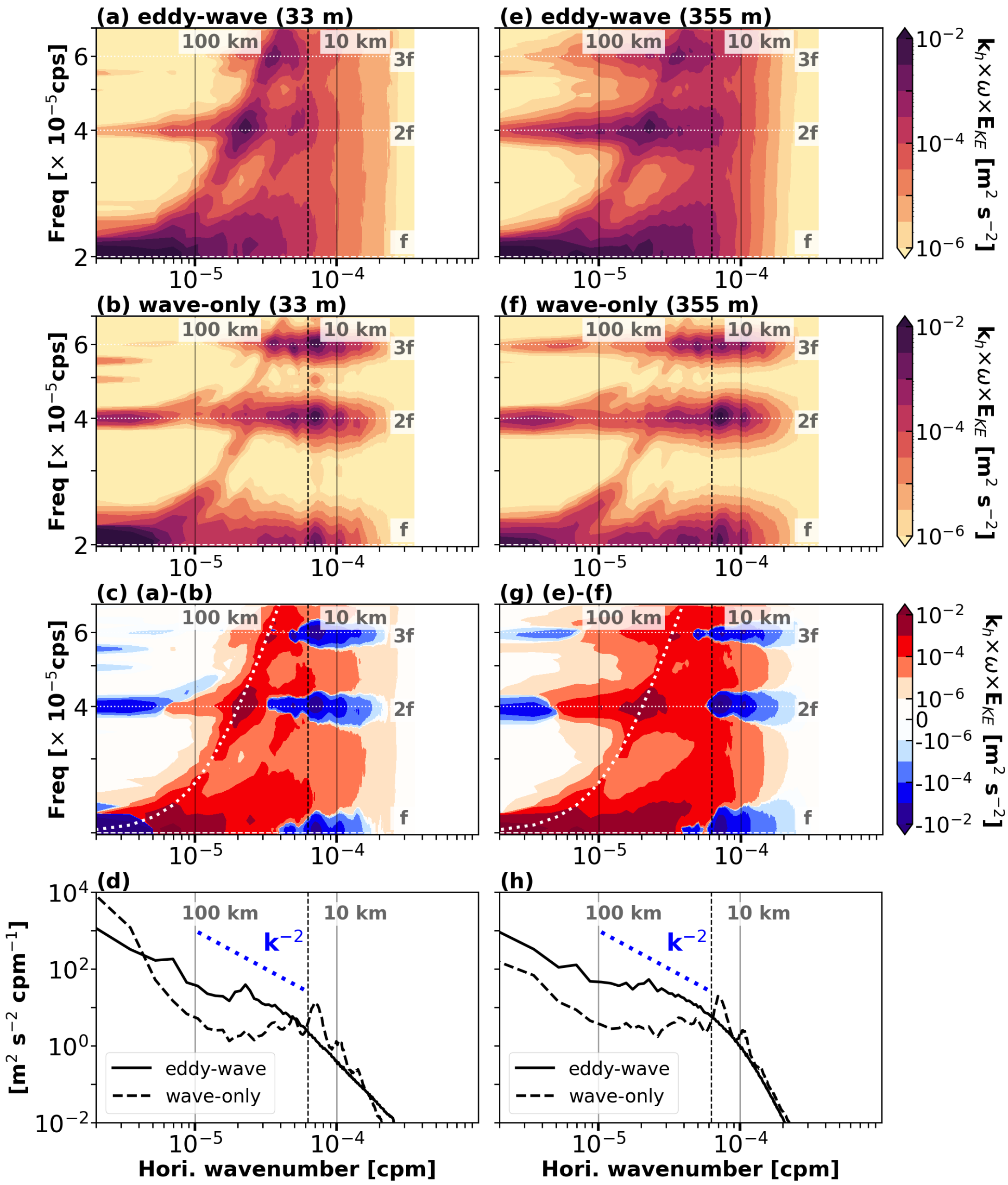

Supplementary Figure 5: Same as Fig. 4 but for the **2 km** simulations.

Supplementary Note 5: Internal wave dispersion relation

The mode-n internal wave dispersion relation is computed following the normal mode expansion (2),

$$\omega_n^2 = f^2 + \frac{N^2 H^2}{n^2 \pi^2} k_h^2, \tag{2}$$

where n is the mode number, ω_n is the frequency of the n-th mode internal wave, f is the Coriolis frequency, N is the stratification, H is the ocean depth, k_h is the horizontal wavenumber.

Supplementary Note 6: Lagrangian filtering window size

Sensitivity tests are performed to choose the advection window size for the Lagrangian filtering (5). We use the frequency spectra at 33 m in the eddy-wave case with 2 km resolution as an example to demonstrate why we select an advection window size of 3 days in the Lagrangian analyses to obtain results shown in Fig. 4. To examine the minimum length of segments required to reproduce the frequency spectrum in the super-inertial range, we divide the original time series into segments using a sliding window of 4-day, 6-day, and 9-day, and average the spectra obtained using these segments. The comparison of

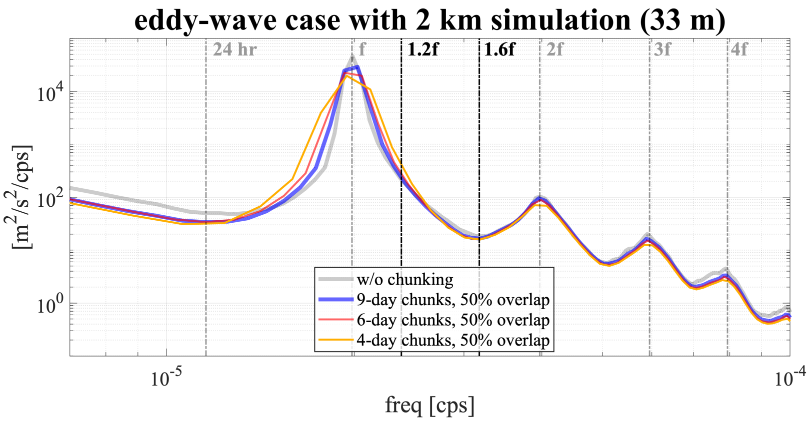

Supplementary Figure 6: The frequency spectra obtained using the 18-day Eulerian time series without chunking data (gray thick line), the 18-day Eulerian time series divided into segments that overlap by 50% using a sliding window of 9 days (purple line), 6 days (red line), and 4 days (orange line) with.

frequency spectra shows that 6-day segments are able to reproduce the spectral peaks at $2f$, $3f$, and $4f$ (Supplementary Fig. 6); for frequencies larger than $1.6f$, the spectral variances of spectra computed using 9-day, 6-day, and 4-day segments are 95%, 90%, and 82% of the spectral variance of the original spectrum, respectively. The frequency spectrum computed using 6-day segments also capture the overall spectral shape and level as well as 9-day segments do (Supplementary Fig. 6); for frequencies larger than $1.2f$, the spectral variances of spectra computed using 9-day, 6-day, and 4-day segments are 100%, 97%, and 94% of the spectral variance of the original spectrum, respectively. We therefore conclude that the minimum length of segments required to reproduce the shape and level of original spectrum is 6-day. The 6-day segments in the Lagrangian filtering are constructed by forward-backward advection using a 3-day advection window size.

Supplementary Note 7: Negative dissipation associated with the under-sampling of viscosity

Here we show the frequency-horizontal-wavenumber cospectrum of kinetic energy dissipation without masking negative values (Supplementary Fig. 7). The negative cospectrum values are primarily seen in the wave-only case at both resolutions. However, most of the negative dissipation cospectrum values

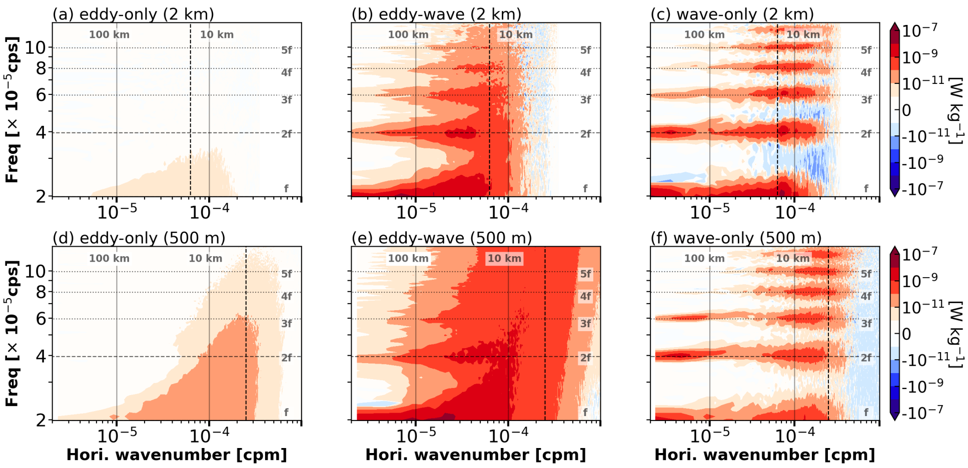

Supplementary Figure 7: Same as Fig. 5 but with the negative cospectrum values.

occur at the scales smaller than the eight grid spacings (indicated by black vertical dashed lines), which are not well resolved because the numerical dissipation starts to take effect. In the resolved wavenumber range, the negative dissipation cospectrum values are more prevalent in the 2 km solutions than in the 500 m solutions, potentially because of the coarser vertical resolution of the 2 km simulations.

The dissipation cospectrum should be sign definite and positive by definition (see equations 1 and 2 in section 4.2). However, the hourly sampling can not resolve temporal variation of the viscosity field within an hour and this sampling bias results in negative dissipation cospectrum values. Here we use the

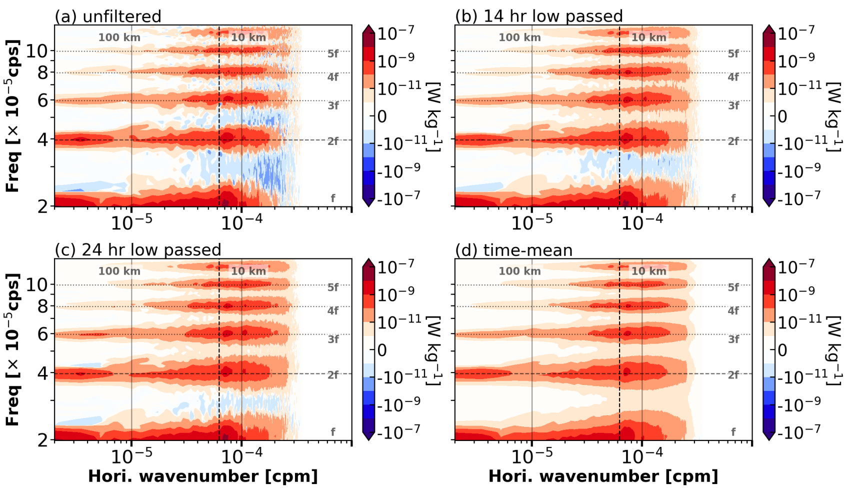

Supplementary Figure 8: The energy dissipation cospectrum in the frequency-horizontal-wavenumber space at 355 m depth in the wave-only case with 2 km resolution, computed using (a) unfiltered viscosity, (b) low-passed viscosity with a cutoff period of 14 hr, (c) low-passed viscosity with a cutoff period of 24 hr, (d) time-mean viscosity over the analysis period.

2km wave-only case as an example to demonstrate that the negative values in the dissipation cospectrum can be removed by low-passing viscosity (Supplementary Fig. 8). When the hourly viscosity field is replaced with a temporally low-passed viscosity, the negative dissipation cospectrum values occupy less frequencies and wavenumbers. When the hourly viscosity time series is replaced with a constant (e.g., the time-mean viscosity over the analysis period), the dissipation cospectrum is positive over all frequencies and wavenumbers.

Supplementary References

[1] Barkan, R., Srinivasan, K., Yang, L., McWilliams, J. C., Gula, J., and Vic, C. (2021). Oceanic Mesoscale Eddy Depletion Catalyzed by Internal Waves. *Geophysical Research Letters*, 48(18).

[2] Gill, A. E. (1984). On the behavior of internal waves in the wakes of storms. *Journal of Physical Oceanography*, 14(7):1129–1151.

[3] Large, W. G., McWilliams, J. C., and Doney, S. C. (1994). Oceanic vertical mixing: A review and a model with a nonlocal boundary layer parameterization. *Reviews of geophysics*, 32(4):363–403.

[4] Renault, L., Molemaker, M. J., McWilliams, J. C., Shchepetkin, A. F., Lemarié, F., Chelton, D., Illig, S., and Hall, A. (2016). Modulation of wind work by oceanic current interaction with the atmosphere. *Journal of Physical Oceanography*, 46(6):1685–1704.

[5] Shakespeare, C. J., Gibson, A. H., Hogg, A. M., Bachman, S. D., Keating, S. R., and Velzeboer, N. (2021). A New Open Source Implementation of Lagrangian Filtering: A Method to Identify Internal Waves in High-Resolution Simulations. *Journal of Advances in Modeling Earth Systems*, 13(10):e2021MS002616.